

ProNav: Proprioceptive Traversability Estimation for Legged Robot Navigation in Outdoor Environments

Mohamed Elnoor, Adarsh Jagan Sathyamoorthy, Kasun Weerakoon, Dinesh Manocha
 Technical report and video can be found at <http://gamma.umd.edu/pronav/>

Abstract— We propose a novel method, ProNav, which uses proprioceptive signals for traversability estimation in challenging outdoor terrains for autonomous legged robot navigation. Our approach uses sensor data from a legged robot’s joint encoders, force, and current sensors to measure the joint positions, forces, and current consumption respectively to accurately assess a terrain’s stability, resistance to the robot’s motion, risk of entrapment, and crash. Based on these factors, we compute the appropriate robot gait to maximize stability, which leads to reduced energy consumption. Our approach can also be used to predict imminent crashes in challenging terrains and execute behaviors to preemptively avoid them. We integrate ProNav with an exteroceptive-based method to navigate dense vegetation and demonstrate our method’s benefits in real-world terrains with dense bushes, high granularity, negative obstacles, etc. Our method shows an improvement up to 50% in terms of success rate and up to 22.5% reduction in terms of energy consumption compared to exteroceptive-based methods.

I. INTRODUCTION

In recent years, autonomous legged robots have found applications in surveillance/monitoring [1], exploration [2], and search and rescue [3]. The key advantage that enables such applications is their superior capabilities in traversing complex terrains, ones that are inaccessible to wheeled and tracked robots.

It is important to develop autonomous methods for navigation in complex terrains, which can be broken down into three major categories: uneven/rocky outdoor terrains, dense vegetation, and granular terrains like sand and mud. The uneven or rocky terrains challenge the robot’s stability as they often lack solid footholds with sudden variations in elevation [4]. Dense vegetation introduces another layer of complexity, presenting risks of entanglement in branches, dried grass, or bushes [5], [6], leading to unstable behaviors such as slipping and tripping. The third category, granular terrains, often leads to the robot’s legs sinking into surfaces like sand or mud due to their deformability under the robot’s weight [7], [8]. Each of these terrain types presents unique difficulties for legged robots, which can affect their navigational capabilities.

To tackle these challenges, the robot must be able to accurately evaluate a terrain’s traversability (a measure of the ease of motion) and then plan its trajectories. Existing methods typically utilize exteroceptive modalities (RGB images, lidar point clouds, and scans) [10], [11], [12], [13], [14] for traversability estimation. Such exteroceptive methods can provide valuable information about the terrain before walking over it. However, these methods experience degradation in perception accuracy in environments with high occlusions, poor illumination, scarce features, etc. For example, the terrain geometry could be occluded by dense vegetation and point clouds could be scattered by tall, thin grass reducing

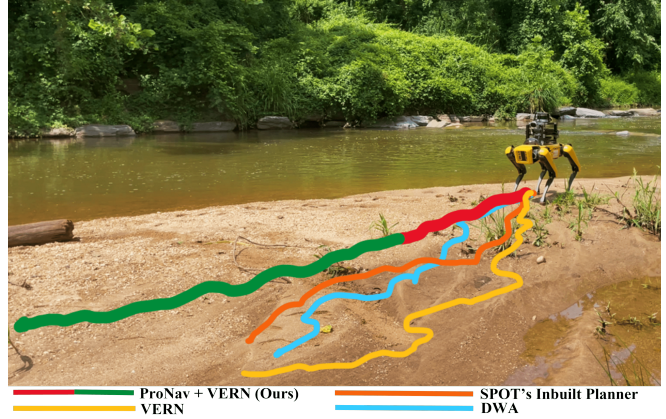


Fig. 1: Comparison of our method ProNav with other methods navigating a Spot robot through a granular terrain: ProNav adapts between two gaits: trot (in red), and amble (in green), Spot’s in-built planner (orange), DWA [9] (sky blue), and VERN [5] (yellow). In this scenario, we observe that only our method successfully reaches its goal due to its quick gait adaptation and accurate proprioception-based traversability estimation.

the LiDAR accuracy. Moreover, certain entities (e.g. negative obstacles such as ditches, and potholes) and changes in a terrain’s properties (dry sand versus wet sand) cannot be accurately detected by such modalities.

To overcome these limitations, several methods have fused exteroception with proprioception to evaluate a terrain’s traversability [15], [16]. Proprioception measures the state of the robot’s joint and body position and force feedback [17], while exteroception sensing measures the state of the environment using sensors such as cameras, LiDAR, etc. Although proprioception cannot provide a look-ahead for the terrain, it more accurately represents the robot’s stability on a terrain since unstable walking behaviors are reflected by significant changes in the positions, forces experienced at certain joints, and high energy consumption. Existing research works on traversability analysis have predominantly focused on environments where the robot encounters slippage [18], [19], [20], and have not handled regions where the robot’s legs could get entangled (e.g. in dense vegetation). Besides that, some terrains, like concrete or asphalt, can be traversed using a single “best” gait, however, this does not apply to all terrains. For example, a grassy terrain may appear uniform but can vary significantly, transitioning from dry to muddy areas with similar visual appearances. Similarly, navigating rocky terrain presents a similar set of challenges as shown in Figure 2. These situations emphasize the importance of an adaptive gait approach informed by proprioceptive signals.



Fig. 2: Force Readings on Rocky Terrain: Images a-c depict sequential RGB captures from the robot's camera, illustrating the progression of the terrain with image a first, followed by b, then c. Image d displays the fluctuations in knee force readings experienced by the robot while traversing the terrain. The high fluctuations represent instances when the robot became unstable. This shows that visually identical terrains could have different stability characteristics.

Main Contributions: To address these limitations, we propose ProNav integrating exteroceptive sensing with proprioception for improved terrain traversability estimation in a variety of environments (rocky, granular, densely vegetated, etc). The proprioceptive signals are measured from a legged robot's joint encoders, force, and current sensors. The novel components of our work include:

- A novel terrain traversability estimation method using only proprioception (joint positions, forces, current consumption) to characterize the stability, and resistance to the robot's motion on a terrain. Our method uses joint proprioceptive signals and battery current for estimating traversability using simple Principal Component Analysis (PCA) within ~ 1 second of walking on a new terrain type using edge computing hardware.
- A novel crash prediction mechanism that can foresee slipping, tripping, and leg entrapment-related crashes. This leads to an improvement of 50% in terms of success rate in densely vegetated regions where all other methods experienced difficulties in reaching the goal.
- A novel gait adaptation approach that selects the appropriate gait leading to increased stability and lower energy consumption while traversing challenging terrains. We highlight the performance of our approach by integrating it with an exteroception-based navigation method for traversing through dense vegetation and rocky and granular terrains.

II. RELATED WORKS

In this section, we discuss the existing methods for estimating terrain traversability, which form the basis of our novel approach. Next, we analyze the existing navigation and planning techniques for legged robots.

A. Perception for Navigation

Autonomous robot navigation in challenging environments requires robots to perceive the real world through their sensors. To this end, robots often incorporate onboard exteroceptive, and proprioceptive sensors. We briefly review the existing work on exteroceptive and proprioceptive perception in the following sub-sections.

1) *Exteroceptive Sensors*: A popular approach is the use of geometry-based methods which reconstruct a 3D representation of the environment by using technologies such as LiDAR or stereo cameras. A typical example of this can be found in [13], where an interpolation technique estimates terrain shape, informing surface characteristics such as height, slope, and roughness. Another approach, as presented in [14], generates a 3D triangle mesh of the environment from a 3D point cloud, which is then input into an online path planner for local navigation. Recently, [21] proposed learning terrain traversability by training a sparse 3D network of occupancy maps. However, these geometry-based methods have limitations, including difficulties with deformable surfaces such as sand, obstacles like tall grass, and the risk of poor estimation [13], [2].

Concurrently, vision-based approaches have seen widespread application in robot perception [10], [11], [12]. Previous work in semantic segmentation categorizes terrain properties into traversable and non-traversable classes. For instance, Guan et al [22] leverage a multi-head vision transformer architecture to segregate the terrain into six distinct categories. Also, traversability classification can be performed using anomaly detection from multi-model images [23]. Even though such vision-based systems perform well under perfect weather conditions, they often result in erroneous classification due to motion blur [24] and lighting changes [25].

Several studies have also explored the potential of sensor fusion for terrain classification [26], [27], [28], [29]. Notably, in [26], geometric and vision-based techniques are used to deliver improved performance. In [28], reliability-aware sensor fusion is performed to mitigate the performance degradation due to cluttered sensing. Recently, [5] proposed VERN, which utilizes a lightweight Siamese network to classify complex outdoor vegetation based on traversability. The method in [30] employs IMU sensor data to learn surface traction, bumpiness, and deformability using an online self-supervised learning strategy. While this approach has shown promising results for a number of terrains, others like rocks and bushes, with irregular texture/structure, were not investigated.

2) *Proprioceptive sensors*: In outdoor environments, exteroceptive sensors could receive noisy data because of factors such as degraded lighting conditions and occlusions. Also, the environment can be extreme and challenging. For instance, the ground could be covered by vegetation (e.g., short/tall grass, bushes) and the robot cannot recognize the terrain type using vision or LiDAR. To overcome such issues, there has been a continuous development in proprioceptive perception [31], [32]. Moreover, proprioception can be coupled with vision in legged robots as in [15], where Fu et al. use the camera to create a cost map around the robot, while the terrain traversability is mainly evaluated based

on proprioceptive feedback. That also helps in avoiding unexpected obstacles such as glass walls. [33] proposed a cross-modal algorithm that uses an RGB camera and shifted proprioception to learn a walking locomotion policy. More recently, Dey et al. [34] leverage the proprioceptive information from a legged robot's joints to predict slip and fall events with high accuracy. However, the robot is operated in a limited number of terrains such as rubble and other uneven, underground terrains, and not in densely vegetated environments. Moreover, their proposed model primarily predicted slipping and tripping and it is not used for navigation. Our novel approach uses proprioceptive feedback and current consumption from the actuators to also detect entanglement in dense vegetation and recover the robot.

B. Outdoor Navigation

Recently, many approaches have been proposed to leverage the agile mobility of legged robots [35], [36] in unstructured outdoor environments, which is challenging for wheeled robots [37]. Some of these works use cost maps to represent the traversability of the environments [38], [39]. Semantic Belief Graph are utilized in [40] to train a policy for trajectory generation in extreme environments. Moreover, a traversability uncertainty-based method is proposed in [41]. In [42], the authors presented a traversability estimator that uses a classifier (or a regressor) neural network based on elevation maps. Silver et al. [43] described an approach based on learning from demonstrations for autonomous navigation in natural terrains. Artplanner [44] is a navigation planner designed for the DARPA Subterranean Challenge that uses geometric reachability checking and a motion cost neural network to compute optimal paths. Proprioceptive feedback is also used in the literature [6], [15], [34]. In [6], Lee et al. utilized proprioceptive feedback to train a robot controller using reinforcement learning. Their approach shows zero-shot capabilities when tested in outdoor settings. However, an inherent limitation of proprioception is its inability to preview terrain features before the robot directly interacts with them. This limitation motivates the integration of ProNav with an exteroceptive-based navigation method, ensuring a more comprehensive navigation strategy.

III. BACKGROUND

In this section, we explain our assumptions, define important notations used, and our problem formulation.

A. Setup and Conventions

We assume a quadrupedal robot with 12 degrees of freedom (DOF), with 2-DOFs in the hip, and 1-DOF in the knee of each leg. We assign numbers 1, 2, 3, and 4 to denote the front-left, front-right, rear-left, and rear-right legs respectively, and i to denote each leg. A robot coordinate frame is established at its center of mass with positive X, Y, Z pointing forward, left, and up respectively. Frames with similar conventions are established at each hip and knee joint. The hip actuators are capable of moving in X and Y directions, and the knee actuator moves along the Z direction. We also measure the positions $p_x^{hip,i}, p_y^{hip,i}, p_z^{knee,i}$, velocity $v_x^{hip,i}, v_y^{hip,i}, v_z^{knee,i}$, and force $f_x^{hip,i}, f_y^{hip,i}, f_z^{knee,i}$ exerted at a time instant t .

Position and velocity data at the joints are measured using encoder sensors, and the forces experienced are measured using the internal tactile sensing mechanism. Finally, we assume that the current drawn ($I(t)$) from the robot's battery can be measured using an ammeter or a current sensor while traversing various terrains. We define $\mathbf{X}_t \in \mathbb{R}^{36}$ as the set of all positions (3), velocities (3), and forces (3) obtained from all four legs of the robot.

Based on our setup and notation, we have formulated the state vector for our traversability estimation method. The state at any given time instant t is represented by a vector that includes joint positions, velocities, forces, and the current drawn from the robot's battery. This state vector is formally defined as:

$$\text{State Vector} = [\mathbf{X}_t \in \mathbb{R}^{36}, I(t) \in \mathbb{R}]$$

Here, \mathbf{X}_t encompasses all positions, velocities, and forces obtained from the four legs of the robot, while $I(t)$ represents the current drawn from the robot's battery.

B. Problem Domain

The focus of our approach is to enhance the navigational capabilities of legged robots traversing through a variety of terrains (e.g. densely vegetated, granular, rocky) using proprioceptive feedback to predict and adapt to changes in surface conditions. In these terrains, the robot's legs could slip, trip, sink, or get entangled. We define a robot crash and briefly explain the factors that cause these unstable phenomena, potentially causing the robot to crash:

- **Robot crash:** A robot falling to the ground which could be caused by one of the following cases:
 - **Poor Foothold:** This causes the robot's feet to slip in rocky or slippery terrains because the robot's feet do not have a firm, flat surface to support themselves on.
 - **Granularity:** This causes the robot's feet to sink into the terrain (e.g. sand, mud, snow) leading to erroneous measurements of joint positions. This could cause the robot's controller to overcompensate to stabilize itself.
 - **Resistance to Motion:** This is typically caused by dense, pliable vegetation that can be passed through (e.g. tall grass and bushes). Additionally, the robot's legs could get entangled with vegetation causing higher resistance to motion.

To traverse various terrains, we assume a legged robot with a locomotion model that can alternate between three gaits: trot, crawl, and amble [34], [35]. Trot is the standard walking gait where the robot walks with two legs on the ground at a time instance, allowing fast movements. It is stable on hard surfaces, with moderate power consumption. On the other hand, during crawl and amble, the robot has three legs on the ground at a time instance, leading to more stable behaviors in uneven, granular, deformable surfaces. Despite their similarities, amble has much higher velocity compared to crawl, which also leads to a high power consumption. Amble helps to traverse through environments with high resistance to motion while also maintaining stability, which also helps handle poor foothold terrains. Similarly, crawl maintains high stability in granular terrains and regions with

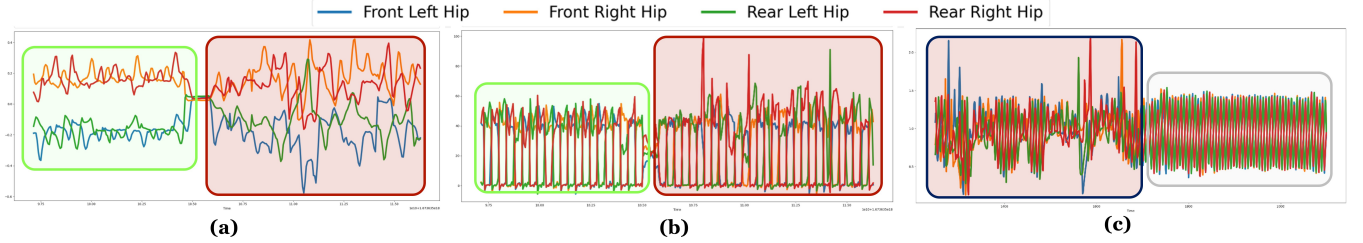


Fig. 3: (a) Changes in the hip x-axis position of the robot while traversing grass (green box), and rocks (brown box). The relatively stable readings during grass traversal contrast the substantial fluctuations seen on the more challenging rocky terrain due to frequent slips. (b) Force exerted by the four actuators associated with the robot's legs while traversing grass (green box), and rocks (brown box). Steady readings observed on stable grass terrain reflect ease of traversal, while the increased volatility and noticeable spikes on the rocky terrain are indicative of increased resistance and unevenness, causing variable load on the actuators. (c) Changes in the hip y-axis position of the robot while traversing dense vegetation (purple box), and concrete (gray box). Fluctuations are observed while traversing dense vegetation due to the legs' entanglement instances. Conversely, a steady and consistent reading is observed during concrete traversal.

poor footholds while consuming minimal power. Based on these definitions, our formulation can be stated as follows,

Formulation III.1. *To adaptively select a stable gait g^* given collision-free, goal-directed velocities (v^*, ω^*) , and a set of proprioceptive signals $\mathbf{Y}_t \subset \mathbf{X}_t$ from a legged robot to improve stability and prevent crashes.*

IV. PRONAV: PROPRIOCEPTION-BASED STABLE NAVIGATION

In this section, we analyze and choose the relevant proprioceptive signals, process them to assess stability and explain our gait adaptation strategy to stabilize the robot.

A. Analysis of Proprioceptive Signals

Our goal is to choose the fewest number of proprioceptive signals that are also excellent indicators of stability. In other words, we want to choose the minimum subset $\mathbf{Y}_t \subset \mathbf{X}_t$, the set of all available proprioceptive signals at time t , such that the terrain traversability is accurately determined.

Hip's Position: Our empirical analysis revealed a strong correlation between the amount of slip on a terrain and the change in hip position along the X-axis and Y-axis. Figure 3 visually represents these changes as the robot navigates three different types of terrain, each representing different levels of traversability: grass, mulch, and rocks.

Knee's force: Sudden peaks in the forces experienced by the robot's knee actuators (Fig. 3) along the Z direction indicate an absence of stable footholds due to unevenness, causing the robot to exert more effort to stabilize itself.

Current Consumption: The amount of current consumed while traversing various terrains at a consistent elevation is proportional to the resistance to motion experienced in each terrain (Fig. 4). Moreover, the robot's gait consistently impacts the current consumption on different terrains following the trend $I^{\text{Amble}} > I^{\text{Trot}} > I^{\text{Crawl}}$.

B. Prepossessing Proprioceptive Signals

Our goal in preprocessing the chosen force and position data is to obtain quantities that change drastically on various terrains, thus indicating their properties. Vectors of the processed data are then analyzed using Principal Component Analysis (PCA).

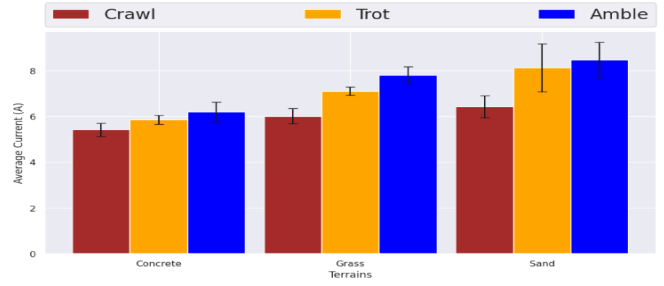


Fig. 4: The average current consumption in amperes, with 95% confidence interval as the robot traverses concrete, grass, and sand. Lower current consumption on concrete indicates efficient traversal. However, higher values on sand highlight increased resistance and energy usage. Additionally, a consistent trend in current consumption is exhibited while using crawl, trot, and amble on various terrains.

1) *Preprocessing Force Data:* At any time instant t , we consider past n samples of $f_z^{knee,i}$ of the i^{th} leg. That is, we consider the vector $[f_z^{knee,i}(t), f_z^{knee,i}(t-1), \dots, f_z^{knee,i}(t-n+1)]$. Next, we obtain the mean force for the i^{th} leg's knee as $\mu_f^i = (\sum_{j=0}^{n-1} f_z^{knee,i}(t-j))/n$, and then the mean force experienced by the robot as a whole as $\mu_f^{rob} = (\sum_{i=1}^4 \mu_f^i)/4$. Finally, we calculate the difference $\Delta_f^i = \mu_f^{rob} - f_z^{knee,i}(t)$ for each leg. As the robot walks on various terrains, $\Delta_f^i < 0$ indicates that the robot has entered a poorly traversable terrain which leads to high knee forces, and $\Delta_f^i > 0$ indicates a highly traversable terrain. To further amplify changes in traversability, we use $\sum_{i=1}^4 \Delta_f^i$, and a counter that denotes the number of spikes in the force experienced, defined as: $count = count + 1$ if $\Delta_f^i < 0, i \in \{1, 2, 3, 4\}$.

2) *Preprocessing Position Data:* At time instant t , we consider the past m samples of $p_{x,i}^{hip}$. For each leg i , we calculate the maximum max_i and minimum min_i values of these m samples and finally calculate $\Omega_{p-x}^{rob}(t) = \sum_{i=1}^4 |max_{i-x} - min_{i-x}|$. Ω_{p-x}^{rob} represents the magnitude of variation in the hip positions along the X direction. Similarly, we obtain Ω_{p-y}^{rob} along the Y direction. A high value of $\Omega_{p-x}^{rob}(t)$ or $\Omega_{p-y}^{rob}(t)$ indicates the unavailability of stable footholds which leads to slippage (e.g. in rocky terrains), or the presence of a granular surface that leads to sinkage.

3) *Processed Input Vector*: We combine the processed quantities in knee forces and hip positions with the current drawn from the robot's battery to construct the input vector $A \in \mathbb{R}^9$ to estimate terrain traversability as,

$$A(t) = [\Delta_f^1, \Delta_f^2, \Delta_f^3, \Delta_f^4, \sum_{i=1}^4 \Delta_f^i, count, \Omega_{p-x}^{rob}, \Omega_{p-y}^{rob}, I]. \quad (1)$$

All the quantities on the left in equation 1 are functions of t . It is omitted for readability.

C. Terrain Traversability Estimation

To estimate a terrain's traversability using our denoised proprioceptive signal, we first apply Principal Component Analysis (PCA) to reduce its 9 dimensions into two principal components. This method allows us to simplify and effectively compare different terrains based on these components. We investigated using a different number of principal components, such as 1 and 3. We discovered that using just one component was insufficient to differentiate between stable terrains, such as concrete, and unstable terrains, like rocks. Additionally, the use of three components did not yield additional insights beyond what was already apparent with the two-component analysis in terms of visualizing distributions for each type of terrain as shown in Figure 5.

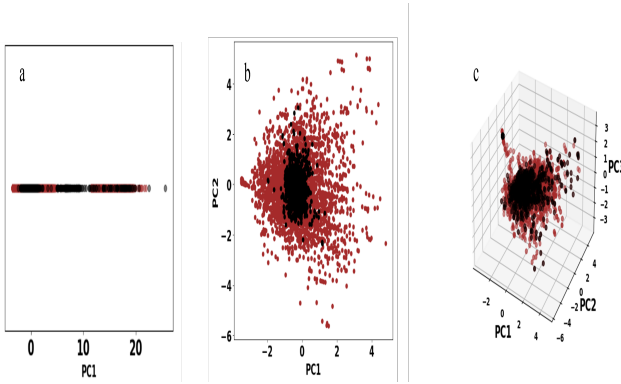


Fig. 5: Terrain Representation with Varying PCA Components: Figure a illustrates the use of 1 component, b shows the use of 2 components, and c displays the use of 3 components. In these figures, brown indicates rocky terrain, while black denotes concrete terrain. Notably, the use of 2 components, as depicted in b, offers a more distinct and clearer representation of the terrains compared to using either 1 or 3 components.

The resulting plots of the first two principal components in Fig. 6 reflect that the variance of the data along the two principal components differentiates stable (low variance) and unstable (high variance) terrains (grass versus sand, and grass versus rocks). Using variances σ_{PC1}^2 and σ_{PC2}^2 , we define the cost of traversing a terrain as,

$$f(\sigma_{PC1}^2, \sigma_{PC2}^2) = \sqrt{\sigma_{PC1}^2 + \sigma_{PC2}^2} \quad (2)$$

Function $f(\cdot)$ implicitly assesses stability and the current/power consumed while traversing a terrain. Furthermore, we observe that the PCA outputs are capable of predicting imminent crashes with noticeable shifts during the moments immediately before and after crashes (see Fig. 6).

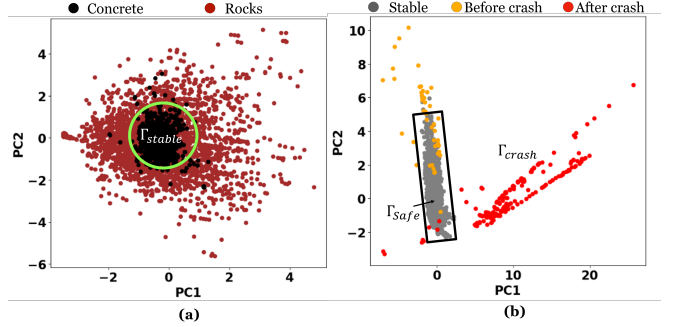


Fig. 6: PCA applied to key proprioceptive metrics (hip actuator position, knee actuator force, and battery current) across different terrains. (a) The variances along the two principal components between concrete (stable) and rocks (unstable terrain). Unstable terrains lead to high variances. During unstable navigation, the robot's proprioceptive signals lie outside the green circle centered at $(0, 0)$ with a radius of Γ_{stable} . (b) The shift in distribution between stable navigation (grey points), before a crash (yellow), and finally after a crash (red). The corners of the Γ_{safe} rectangle corners from the bottom left corner and moving clockwise: $(-1.2, -2.25)$, $(-3, 5)$, $(0.5, 15)$, and $(2.5, -2.35)$. If the robot's proprioceptive signals lie outside the rectangle Γ_{safe} , the robot is headed towards a crash.

D. Assessment of Stability

Although $f(\cdot)$ indicates the *severity* of a terrain's lack of stability, it does not indicate the factors (poor foothold, granularity, resistance to motion) responsible for it. To analyze stability, we utilize raw $p_x^{hip,i}$, and $p_y^{hip,i}$ values. We found that $p_y^{hip,i}$ is more indicative of poor foothold and motion resistance, like in bushes. Conversely, granular terrain causes more changes in $p_x^{hip,i}$. Therefore, we define a cost function relating the robot's stable gaits with these stability factors as:

$$h(gait) = \begin{cases} \frac{1}{\sum_{i=1}^4 p_y^{hip,i}} & \text{if gait} = \text{Amble} \\ \frac{1}{\sum_{i=1}^4 |p_x^{hip,i} - \epsilon_x^{hip,i}|} & \text{if gait} = \text{Crawl.} \end{cases} \quad (3)$$

where $\epsilon_x^{hip,i}$ is a predefined threshold for i^{th} hip. $h(\cdot)$ is designed to return a low-cost value for a gait if it effectively resolves the primary factors affecting stability.

E. Stable Gait Adaptation

Our method prioritizes stability in terrain traversal. Based on the stability assessment $h(\cdot)$ and the severity indicator $f(\cdot)$, we determine the most suitable gait, g^* , as follows:

$$g^* = \underset{g \in \{\text{Amble, Crawl}\}}{\operatorname{argmin}} h(g) \text{ if } f(\cdot) > \Gamma_{stable}. \quad (4)$$

$$g^* = \text{None}, (v^*, \omega^*) = (0, 0) \text{ if } f(\cdot) \text{ is outside } \Gamma_{x,safe}. \quad (5)$$

Here, Γ_{stable} denotes stability thresholds. Γ_{safe} , Γ_{crash} denote safe and potential crash areas, respectively. An example of Γ_{stable} , Γ_{safe} and Γ_{crash} is shown in Fig. 6. When the magnitude of $f(\cdot)$ goes outside of Γ_{safe} , it cannot be stabilized using any gait. Therefore, ProNav prevents a crash by halting the robot until $f(\cdot)$ is within Γ_{crash} .

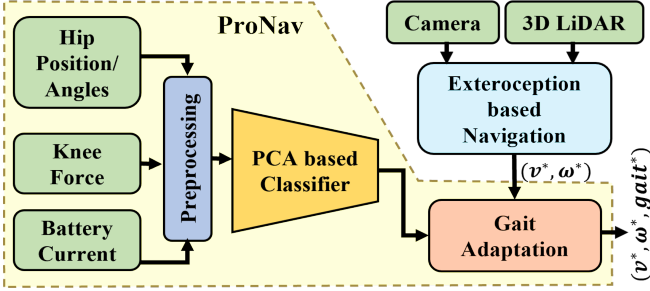


Fig. 7: ProNav System Architecture for improved gait and velocities. We utilize hip x-axis position, knee force, and battery as our proprioceptive signals. Our PCA-based classifier estimates the traversability of the terrain. The gait adaptation selects the improved gait for stability. The camera and lidar are used with the integrated exteroception-based planner for obstacle avoidance.

Algorithm 1 ProNav: Proprioception-based Traversability Estimation

```

1: Initialize:  $\mathbf{Y}_t \subset \mathbf{X}_t$ , PCA parameters,  $\Gamma_{stable}$ ,  $\Gamma_{crash}$ ,  $\Gamma_{safe}$ ,  $n, m$ 
2: for each time  $t$  do
3:   Extract positions, velocities, and forces to  $\mathbf{X}_t$ 
4:   Obtain  $\mathbf{Y}_t$  from  $\mathbf{X}_t$ 
5:    $\mu_f^i, \mu_f^{rob} \leftarrow \mathbf{Y}_t$  // Preprocessing
6:   for each leg  $i$  do
7:     Calculate:  $\Delta_f^i$ , update count based on  $\Delta_f^i$ 
8:   end for
9:    $\Omega_{p-x/y}^{rob}(t) \leftarrow \sum_{i=1}^4 |max_{i-x/y} - min_{i-x/y}|$ 
10:   $A(t) \leftarrow$  Eq. 1
11:   $\sigma_{PC1}^2, \sigma_{PC2}^2 \leftarrow PCA(A(t))$ 
12:   $f(\cdot) \leftarrow f(\sigma_{PC1}^2, \sigma_{PC2}^2)$ 
13:  if  $f(\cdot) > \Gamma_{stable}$  then
14:    Evaluate  $h(gait)$ 
15:     $g^* \leftarrow \underset{g \in \{\text{Amble, Crawl}\}}{\operatorname{argmin}} h(g)$ 
16:    if  $f_x(\cdot)$  is outside  $\Gamma_{safe}$  then
17:       $g^* \leftarrow \text{None}$ 
18:    end if
19:  end if
20: end for

```

F. Algorithm

The designed algorithm for our navigation system is described in algorithm 1.

This approach enables the robot to safely navigate varied terrains while considerably minimizing the risk of crashes due to slippage, sinkage, and leg entrapments.

G. ProNav + Exteroception

Although proprioceptive modalities help to estimate the traversability of the terrain the robot is walking on, they lack *look-ahead* capability (whenever terrain is visible) that exteroceptive sensing affords. That is because the traversability of terrains ahead of the robot cannot be assessed using past and current proprioceptive data. Therefore, fusing exteroception and proprioception helps bring out the best of both worlds.

ProNav can be easily combined with any navigation method that uses exteroceptive sensing such as RGB images, 3D point clouds, etc. An overview of such a hybrid architecture is shown in Fig. 7. The collision-free, goal-directed

velocities (v^*, ω^*) are extracted from an exteroception-based planner [9], [28], [5], and the gait evaluated to be the most stable for the current scenario by ProNav (equation 4) are used by the robot. (v^*, ω^*) ensures the robot's safety in terms of avoiding solid obstacles, and ProNav ensures walking stability.

V. RESULTS AND ANALYSIS

This section outlines ProNav's implementation, our chosen evaluation parameters, the varied test environments, and comparisons with other methods.

A. Robot Setup and Dataset

Our approach is implemented on a Spot robot, a 12-degree-of-freedom (DOF) quadruped from Boston Dynamics. The robot provides joint feedback from its 12 actuators and the battery current data during its operation. Our data collection was carried out in the diverse environments of the University of Maryland College Park campus, on different terrains including concrete, asphalt, grass, rocks, sand, bushes, and mulch. The resulting dataset represents approximately 7 hours of operation, during which the joint feedback and battery current were continuously recorded. This collection presents a detailed account of Spot's interaction with its environment and its energy consumption metrics.

B. Comparison Methods

We combine ProNav with VERN [5] and compare its performance with three purely exteroceptive navigation techniques:

- **Spot's in-built planner:** Uses 360° RGB-D cameras to detect and avoid obstacles.
- **Dynamic Window Approach (DWA)** [9]: Uses 2D lidar scans for obstacle avoidance.
- **VERN** [5]: Uses RGB images and 3D point clouds to differentiate pliable vegetation from solid obstacles and traverse vegetated environments.

Additionally, we also perform ablation studies by removing the joint positions and current components from our input to our PCA-based classifier.

C. Evaluation Metrics

- **Success Rate:** The ratio of successful navigation trials where the robot was able to reach its goal without freezing or colliding with obstacles.
- **Mean power consumption:** The amount of power (in Watts) consumed from the robot's battery averaged over all trials.
- **Mean Velocity:** The robot's average velocity along its trajectory as it traverses various surfaces.
- **Time to Goal:** The robot's average time to reach its goal in the successful trials.
- **Vibration Cost:** The cumulative sum of deviations in hip joint positions from a stable reference, measured at each time instant t . Deviations for each hip joint j in the x- and y-axes are calculated as follows:

$$\delta_j(t) = \begin{cases} \left| p^j(t) - \min(p_{ref}^j) \right| & \text{if } p^j(t) < \min(p_{ref}^j), \\ \left| p^j(t) - \max(p_{ref}^j) \right| & \text{if } p^j(t) > \max(p_{ref}^j). \end{cases}$$

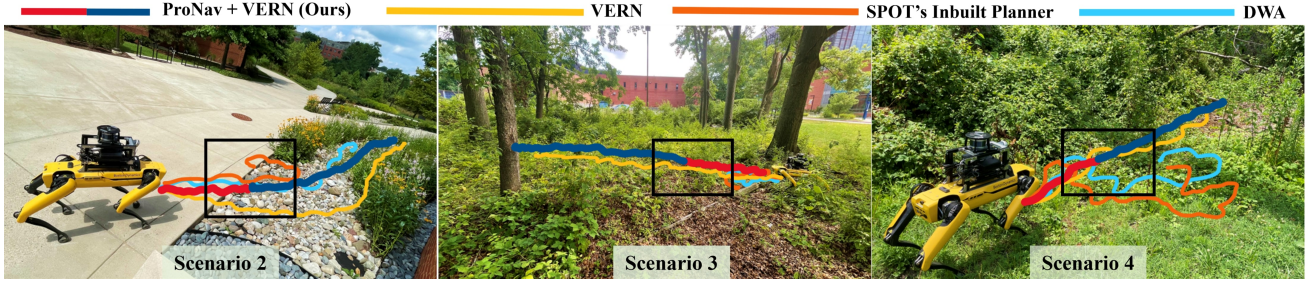


Fig. 8: Spot navigating in different outdoor terrains using: ProNav(trot: red, amble: dark blue), Spot’s in-built planner (orange), DWA (sky blue), and VERN (yellow). The black box shows the gait switching location. We observe that ProNav chooses the appropriate gait and velocities based on terrain traversability, leading to better success rates, lower power consumption, and vibration cost.

Here, $p^j(t)$ is the position of joint j at time t , and p_{ref}^j represents reference positions from a stable terrain (for this work concrete is considered a stable terrain). The total Vibration Cost at time t is then computed as:

$$\text{Vibration Cost}(t) = \sum_j \delta_j(t).$$

- **IMU Energy Density** : The mean of the aggregated squared acceleration values measured by the IMU sensors across the x, y, and z axes, calculated over the successful trials.

The relevant equations implemented are adopted from [45]:

$$E_i = \sum_{n=1}^N a_i^2, \quad (6)$$

$$E_{\text{Total}} = E_{ax} + E_{ay} + E_{az}, \quad (7)$$

where a_i represents one of the three acceleration signals (x, y, and z axes), and N is the IMU readings along the trajectory.

D. Test Scenarios

- **Scenario 1:** Granular terrains (small rocks and sand).
- **Scenario 2:** Concrete, rocks, and vegetation.
- **Scenario 3:** Sparse tall grass, fallen logs, and trees.
- **Scenario 4:** Dense vegetation and bushes.

E. Analysis and Discussion

In this section, we evaluate qualitatively and quantitatively the performance of our method and compare it with other methods. Figure 8 provides a visual representation of the trajectories in different terrains. Our method showcases its superiority in navigating through granular (Fig. 1), rocks (Fig. 8.a), unstructured terrains (Fig. 8.b), and dense vegetation (Fig. 8.c). Notably, our method adapts by choosing crawl on sand (scenario 1) and amble in other scenarios where poor footholds and resistance to motion dominates. In comparison, the lidar-based DWA method and Spot’s builtin system struggle in vegetation-rich scenarios (2,3 and 4). That’s due to their default gait “trot”, which causes leg entanglement in vegetation. That’s evident in their low success rate in such scenarios. Meanwhile, VERN generally navigates efficiently with a high success rate (scenarios 2 and 3), but there are instances where it encounters failures, primarily due to similar entanglements. A relatively lower

TABLE I: Navigation performance of other methods compared to other methods using four different metrics. We observe that ProNav’s performance is the highest in success rate. Additionally, our method leads to the lowest power consumption and vibration cost.

Metrics	Method	Scen. 1	Scen. 2	Scen. 3	Scen. 4
Success Rate (%)	In-built system	40	10	10	-
	DWA[9]	60	30	20	-
	VERN[5]	90	70	80	60
	w/o current+VERN	100	70	60	50
	w/o position+VERN	100	80	70	70
Mean Power Consumption (watt)	ProNav+VERN	100	80	100	90
	In-built system	488	451	523	-
	DWA[9]	496	402	392	-
	VERN[5]	475	371	350	446
	w/o current+VERN	358	362	352	400
Mean Velocity (m/s)	w/o position+VERN	375	342	351	414
	ProNav+VERN	368	341	348	370
	In-built system	0.42	0.33	0.30	-
	DWA[9]	0.46	0.35	0.32	-
	VERN[5]	0.45	0.49	0.33	0.30
Time to Goal (seconds)	w/o current+VERN	0.30	0.43	0.34	0.41
	w/o position+VERN	0.22	0.50	0.31	0.33
	ProNav+VERN	0.28	0.39	0.25	0.32
	In-built system	19.34	24.24	27.06	-
	DWA[9]	17.34	23.54	25.03	-
Vibration Cost	VERN[5]	19.25	16.12	24.39	26.63
	w/o current+VERN	27.08	18.72	23.2	19.59
	w/o position+VERN	35.25	16.62	26.12	24.29
	ProNav+VERN	26.47	20.82	29.04	25.34
	In-built system	67.2	56.7	54.1	-
IMU Energy Density	DWA[9]	45.1	38.1	22.3	-
	VERN[5]	23.1	23.9	11.7	25.1
	w/o current+VERN	20.8	12.6	90.2	5.4
	w/o position+VERN	44.4	2.6	13.3	10.9
	ProNav+VERN	15.2	2.7	8.1	4.8
	In-built system	52349	30766	49597	-
	DWA[9]	49102	27211	22008	-
	VERN[5]	57636	25253	16786	34712
	w/o current+VERN	26583	17002	25053	23341
	w/o position+VERN	28742	16504	12035	19203
	ProNav+VERN	27332	11755	14081	17644

success rate is observed in scenario 4, where the vegetation is dense. On the other hand, our method achieves the highest success rate in all scenarios with its gait adaption. Compared to the second best method (VERN), our method improves the success rate by 11.11% in scenario 1, 14.28% in scenario 2, 25% in scenario 3, and 50% in scenario 4, as shown in Table I. We compute the success rate improvement using the following equation:

$$\text{Success Rate Improvement (\%)} = \left(\frac{SR_{\text{ours}} - SR_{2\text{nd}}}{SR_{2\text{nd}}} \right) \times 100 \quad (8)$$

Where:

- SR_{ours} represents the success rate of our proposed method.
- SR_{2nd} is the success rate of the second-best method.

We observe that our method results in the lowest power consumption across all the tested terrains. This efficiency is a result of its capability to assess stability and its superiority in gait selection. VERN, while comparable in certain scenarios, has increased power consumption in the fourth scenario due to its default trot gait leading to more entanglements and consequent motion resistance.

Moreover, our method consistently records the lowest vibration levels (in terms of the vibration cost and the IMU energy density metrics). In contrast, Spot’s in-built system and DWA[9] experience higher vibration costs due to sinkage (scenario 1), slippage (scenario 2), and motion resistance (scenario 3). In the mean velocity metric, ProNav shows a reduced pace, particularly during the gait switch to crawl in scenario 1. ProNav’s time to goal is comparable to all other methods, except in scenario 1, where the exteroceptive-based methods preferred using a fast gait but with a high vibration cost.

Ablation Study on Proprioceptive Signals: Our ablation analysis focused on two proprioceptive signals of ProNav: current drawn from the battery and hip joints’ positions. In our evaluations (Table I), omitting battery current resulted in notably delayed or incorrect traversability estimations, notably impacting power consumption and vibration costs, especially evident in scenario 4 in dense vegetation. Removing hip joints’ positions also hindered performance but to a lesser extent. Despite their relative performance, neither ablated configuration could exceed the performance of the fully integrated ProNav system. We didn’t remove the knee force for our ablation study, because there’s no PCA cluster without it which hinders the comparison.

Table II shows navigation comparisons when using a single stable gait (crawl or amble) as well as ProNav with its adaptive gait adjustment. We observe that crawl gait has the lowest power consumption and vibration levels compared to the amble gait. However, its application in dense vegetation presents challenges; the robot moves slowly, leading to its legs getting entangled with the vegetation. These challenges are experienced in scenario 4 for the crawl gait, where we note elevated power consumption and vibration levels alongside a significantly diminished velocity. In contrast, the amble gait consistently achieves superior velocities relative to crawl and ProNav. Also, it has high mean power consumption which reduces the risk of entanglement and consequently lower vibration cost. ProNav on the other hand provides the best trade-off between the average power consumption, vibration cost and mean velocity.

VI. CONCLUSION, LIMITATIONS & FUTURE WORK

We present ProNav, a new method that uses proprioceptive data to evaluate terrain’s traversability in real time for legged robots. Our method optimizes robotic gait selection for improved stability and reduced energy consumption. Also, the inclusion of an advanced crash prediction system ensures safer and more efficient navigation. We also combined ProNav with an exteroceptive-based navigation method, which improved its performance. We validate our

TABLE II: Navigation performance while using only stable gaits, crawl, and amble. ProNav adaptively selects the appropriate gait based on the estimated terrain traversability and stability assessment.

Metrics	Method	Scen. 1	Scen. 2	Scen. 3	Scen. 4
Mean Power Consumption (watt)	Crawl	375	367	379	494
	Amble	430	375	415	416
	ProNav	368	341	348	370
Mean Velocity (m/s)	Crawl	0.28	0.24	0.14	0.02
	Amble	0.34	0.57	0.27	0.58
	ProNav	0.29	0.39	0.25	0.44
Time to Goal (seconds)	Crawl	29.78	33.83	57.24	73.26
	Amble	23.52	14.03	29.25	18.82
	ProNav	26.47	20.82	29.04	25.34
Vibration cost	Crawl	17.3	34.1	44.1	35
	Amble	26.4	23.1	3.15	3.6
	ProNav	15.2	2.7	8.1	8.8
IMU Energy Density	Crawl	16355	23934	21555	36754
	Amble	33627	19225	8097	15203
	ProNav	27332	11755	14081	17644

method in different outdoor environments and provide a detailed comparison with other navigational methods.

However, ProNav has some limitations. It can only assess the stability of the terrain the robot is currently on. This could lead to failures and crashes in extreme environments. To solve this, we are considering adding other sensor modalities (e.g. RGB, thermal, or hyperspectral images) that can provide meaningful lookahead for the robot. We would also like to investigate techniques to improve crash prevention, adapting our approach to more diverse environments and situations where halting is insufficient to prevent a crash.

REFERENCES

- [1] Z. Chen, T. Fan, X. Zhao, J. Liang, C. Shen, H. Chen, D. Manocha, J. Pan, and W. Zhang, “Autonomous social distancing in urban environments using a quadruped robot,” *IEEE Access*, vol. 9, pp. 8392–8403, 2021.
- [2] S. B. Goldberg, M. W. Maimone, and L. Matthies, “Stereo vision and rover navigation software for planetary exploration,” in *Proceedings, IEEE aerospace conference*, vol. 5. IEEE, 2002, pp. 5–5.
- [3] C. D. Bellicoso, M. Bjelonic, L. Wellhausen, K. Holtmann, F. Günther, M. Tranzatto, P. Fankhauser, and M. Hutter, “Advances in real-world applications for legged robots,” *Journal of Field Robotics*, vol. 35, no. 8, pp. 1311–1326, 2018.
- [4] E. Tennakoon, T. Peynot, J. Roberts, and N. Kottege, “Probe-before-step walking strategy for multi-legged robots on terrain with risk of collapse,” in *2020 IEEE International Conference on Robotics and Automation (ICRA)*. IEEE, 2020, pp. 5530–5536.
- [5] A. J. Sathyamoorthy, K. Weerakoon, T. Guan, M. Russell, D. Conover, J. Pusey, and D. Manocha, “VERN: Vegetation-aware robot navigation in dense unstructured outdoor environments,” *arXiv preprint arXiv:2303.14502*, 2023.
- [6] J. Lee, J. Hwangbo, L. Wellhausen, V. Koltun, and M. Hutter, “Learning quadrupedal locomotion over challenging terrain,” *Science robotics*, vol. 5, no. 47, p. eabc5986, 2020.
- [7] D. Han, R. Zhang, H. Zhang, Z. Hu, and J. Li, “Mechanical performances of typical robot feet intruding into sands,” *Energies*, vol. 13, no. 8, p. 1867, 2020.
- [8] H. Kolenbach, C. Bärtschi, L. Wellhausen, R. Grandia, and M. Hutter, “Haptic inspection of planetary soils with legged robots,” *IEEE Robotics and Automation Letters*, vol. 4, no. 2, pp. 1626–1632, 2019.
- [9] D. Fox, W. Burgard, and S. Thrun, “The dynamic window approach to collision avoidance,” *IEEE Robotics & Automation Magazine*, vol. 4, no. 1, pp. 23–33, 1997.
- [10] S. Fahmi, V. Barasuol, D. Esteban, O. Villarreal, and C. Semini, “Vital: Vision-based terrain-aware locomotion for legged robots,” *IEEE Transactions on Robotics*, 2022.

[11] A. Agarwal, A. Kumar, J. Malik, and D. Pathak, "Legged locomotion in challenging terrains using egocentric vision," in *Conference on Robot Learning*. PMLR, 2023, pp. 403–415.

[12] Y. Hu, B. Chen, and H. Lipson, "Egocentric visual self-modeling for legged robot locomotion," *arXiv preprint arXiv:2207.03386*, 2022.

[13] D. B. Gennery, "Traversability analysis and path planning for a planetary rover," *Autonomous Robots*, vol. 6, pp. 131–146, 1999.

[14] S. Pütz, T. Wiemann, J. Sprickerhof, and J. Hertzberg, "3d navigation mesh generation for path planning in uneven terrain," *IFAC-PapersOnLine*, vol. 49, no. 15, pp. 212–217, 2016.

[15] Z. Fu, A. Kumar, A. Agarwal, H. Qi, J. Malik, and D. Pathak, "Coupling vision and proprioception for navigation of legged robots," in *Proceedings of the IEEE/CVF Conference on Computer Vision and Pattern Recognition*, 2022, pp. 17273–17283.

[16] T. Homberger, L. Wellhausen, P. Fankhauser, and M. Hutter, "Support surface estimation for legged robots," in *2019 International Conference on Robotics and Automation (ICRA)*. IEEE, 2019, pp. 8470–8476.

[17] A. H. Al-dabbagh and R. Ronsse, "A review of terrain detection systems for applications in locomotion assistance," *Robotics and Autonomous Systems*, vol. 133, p. 103628, 2020.

[18] J. Carius, R. Ranftl, V. Koltun, and M. Hutter, "Trajectory optimization for legged robots with slipping motions," *IEEE Robotics and Automation Letters*, vol. 4, no. 3, pp. 3013–3020, 2019.

[19] S. Teng, M. W. Mueller, and K. Sreenath, "Legged robot state estimation in slippery environments using invariant extended kalman filter with velocity update," in *2021 IEEE International Conference on Robotics and Automation (ICRA)*. IEEE, 2021, pp. 3104–3110.

[20] D. W. Haldane, P. Fankhauser, R. Siegwart, and R. S. Fearing, "Detection of slippery terrain with a heterogeneous team of legged robots," in *2014 IEEE International Conference on Robotics and Automation (ICRA)*. IEEE, 2014, pp. 4576–4581.

[21] J. Frey, D. Hoeller, S. Khattak, and M. Hutter, "Locomotion policy guided traversability learning using volumetric representations of complex environments," in *2022 IEEE/RSJ International Conference on Intelligent Robots and Systems (IROS)*. IEEE, 2022, pp. 5722–5729.

[22] T. Guan, D. Kothandaraman, R. Chandra, A. J. Sathyamoorthy, K. Weerakoon, and D. Manocha, "Ga-nav: Efficient terrain segmentation for robot navigation in unstructured outdoor environments," *IEEE Robotics and Automation Letters*, vol. 7, no. 3, pp. 8138–8145, 2022.

[23] L. Wellhausen, R. Ranftl, and M. Hutter, "Safe robot navigation via multi-modal anomaly detection," *IEEE Robotics and Automation Letters*, vol. 5, no. 2, pp. 1326–1333, 2020.

[24] H. Seok and J. Lim, "Rovins: Robust omnidirectional visual inertial navigation system," *IEEE Robotics and Automation Letters*, vol. 5, no. 4, pp. 6225–6232, 2020.

[25] M. Aladem, S. Baek, and S. A. Rawashdeh, "Evaluation of image enhancement techniques for vision-based navigation under low illumination," *Journal of Robotics*, vol. 2019, 2019.

[26] F. Schilling, X. Chen, J. Folkesson, and P. Jensfelt, "Geometric and visual terrain classification for autonomous mobile navigation," in *2017 IEEE/RSJ International Conference on Intelligent Robots and Systems (IROS)*. IEEE, 2017, pp. 2678–2684.

[27] D. Wisth, M. Camurri, and M. Fallon, "Vilens: Visual, inertial, lidar, and leg odometry for all-terrain legged robots," *IEEE Transactions on Robotics*, 2022.

[28] K. Weerakoon, A. J. Sathyamoorthy, J. Liang, T. Guan, U. Patel, and D. Manocha, "Graspe: Graph based multimodal fusion for robot navigation in unstructured outdoor environments," *arXiv preprint arXiv:2209.05722*, 2022.

[29] A. E. B. Velasquez, V. A. H. Higuti, M. V. Gasparino, A. N. Sivakumar, M. Becker, and G. Chowdhary, "Multi-sensor fusion based robust row following for compact agricultural robots," *arXiv preprint arXiv:2106.15029*, 2021.

[30] A. J. Sathyamoorthy, K. Weerakoon, T. Guan, J. Liang, and D. Manocha, "Terrapn: Unstructured terrain navigation using online self-supervised learning," in *2022 IEEE/RSJ International Conference on Intelligent Robots and Systems (IROS)*. IEEE, 2022, pp. 7197–7204.

[31] T. Miki, J. Lee, J. Hwangbo, L. Wellhausen, V. Koltun, and M. Hutter, "Learning robust perceptive locomotion for quadrupedal robots in the wild," *Science Robotics*, vol. 7, no. 62, p. eabk2822, 2022.

[32] T. Haserbek, Z. Wen, X. Xie, P. Zhao, and W. An, "Model-free end-to-end learning of agile quadrupedal locomotion over challenging terrain," in *2022 IEEE International Conference on Real-time Computing and Robotics (RCAR)*. IEEE, 2022, pp. 699–703.

[33] A. Loquercio, A. Kumar, and J. Malik, "Learning visual locomotion with cross-modal supervision," in *2023 IEEE International Conference on Robotics and Automation (ICRA)*. IEEE, 2023, pp. 7295–7302.

[34] S. Dey, D. Fan, R. Schmid, A. Dixit, K. Otsu, T. Touma, A. F. Schilling, and A.-A. Agha-Mohammadi, "Prepare: Predictive proprioception for agile failure event detection in robotic exploration of extreme terrains," in *2022 IEEE/RSJ International Conference on Intelligent Robots and Systems (IROS)*. IEEE, 2022, pp. 4338–4343.

[35] J. Truong, A. Zitkovich, S. Chernova, D. Batra, T. Zhang, J. Tan, and W. Yu, "Indoor-to-outdoor real: Learning to navigate outdoors without any outdoor experience," *arXiv preprint arXiv:2305.01098*, 2023.

[36] S. Gangapurwala, M. Geisert, R. Orsolino, M. Fallon, and I. Havoutis, "Rloc: Terrain-aware legged locomotion using reinforcement learning and optimal control," *IEEE Transactions on Robotics*, vol. 38, no. 5, pp. 2908–2927, 2022.

[37] P. Biswal and P. K. Mohanty, "Development of quadruped walking robots: A review," *Ain Shams Engineering Journal*, vol. 12, no. 2, pp. 2017–2031, 2021.

[38] D. V. Lu, D. Hershberger, and W. D. Smart, "Layered costmaps for context-sensitive navigation," in *2014 IEEE/RSJ International Conference on Intelligent Robots and Systems*. IEEE, 2014, pp. 709–715.

[39] T. Overbye and S. Saripalli, "Path optimization for ground vehicles in off-road terrain," in *2021 IEEE International Conference on Robotics and Automation (ICRA)*. IEEE, 2021, pp. 7708–7714.

[40] M. F. Ginting, S.-K. Kim, O. Peltzer, J. Ott, S. Jung, M. J. Kochenderfer, and A.-a. Agha-mohammadi, "Safe and efficient navigation in extreme environments using semantic belief graphs," *arXiv preprint arXiv:2304.00645*, 2023.

[41] J. Guzzi, R. O. Chavez-Garcia, L. M. Gambardella, and A. Giusti, "On the impact of uncertainty for path planning," in *2019 International Conference on Robotics and Automation (ICRA)*. IEEE, 2019, pp. 5929–5935.

[42] R. O. C. García, M. A. Estrada, M. Ebrahimi, F. Zuppichini, L. M. Gambardella, A. Giusti, and A. J. Ijspeert, "Gait-dependent traversability estimation on the k-rock2 robot," in *2022 26th International Conference on Pattern Recognition (ICPR)*. IEEE, 2022, pp. 4204–4210.

[43] D. Silver, J. A. Bagnell, and A. Stentz, "Learning from demonstration for autonomous navigation in complex unstructured terrain," *The International Journal of Robotics Research*, vol. 29, no. 12, pp. 1565–1592, 2010.

[44] L. Wellhausen and M. Hutter, "Artplanner: Robust legged robot navigation in the field," *arXiv preprint arXiv:2303.01420*, 2023.

[45] P. Try and M. Gebhard, "A vibration sensing device using a six-axis imu and an optimized beam structure for activity monitoring," *Sensors*, vol. 23, no. 19, p. 8045, 2023.